Journal of Biomolecular NMR (2006) 36:235–249
DOI 10.1007/s10858-006-9087-9

Article

Impact of static and dynamic A-form heterogeneity on the determination of RNA global structural dynamics using NMR residual dipolar couplings

Catherine Musselman[a], Stephen W. Pitt[b], Kush Gulati[a], Lesley L. Foster[a], Ioan Andricioaei[a] & Hashim M. Al-Hashimi[a,*]

[a]*Department of Chemistry, Biophysics Research Division, & Program in Bioinformatics, The University of Michigan, 930 North University Avenue, Ann Arbor, MI 48109-1055, USA;* [b]*Johnson & Johnson Inc, 199 Grandview Road, Skillman, NJ 08558, USA*

Received 10 July 2006; Accepted 6 September 2006

Key words: adaptive recognition, alignment tensor error, idealized A-form helix, rdc, RNA structure, spin relaxation

Abstract

We examined how static and dynamic deviations from the idealized A-form helix propagate into errors in the principal order tensor parameters determined using residual dipolar couplings (rdcs). A 20-ns molecular dynamics (MD) simulation of the HIV-1 transactivation response element (TAR) RNA together with a survey of spin relaxation studies of RNA dynamics reveals that pico-to-nanosecond local motions in non-terminal Watson–Crick base-pairs will uniformly attenuate base and sugar one bond rdcs by ~7%. Gaussian distributions were generated for base and sugar torsion angles through statistical comparison of 40 RNA X-ray structures solved to < 3.0 Å resolution. For a typical number (≥11) of one bond C–H base and sugar rdcs, these structural deviations together with rdc uncertainty (1.5 Hz) lead to average errors in the magnitude and orientation of the principal axis of order that are < 9% and < 4°, respectively. The errors decrease to < 5% and < 4° for ≥17 rdcs. A protocol that allows for estimation of error in A-form order tensors due to both angular deviations and rdc uncertainty (Aform-RDC) is validated using theoretical simulations and used to analyze rdcs measured previously in TAR in the free state and bound to four distinct ligands. Results confirm earlier findings that the two TAR helices undergo large changes in both their mean relative orientation and dynamics upon binding to different targets.

Introduction

The A-form double helix is the most abundant structural element in RNA that reoccurs in similar form in a variety of structural contexts (Moore, 1999; Neidle, 1999). The overall architecture of RNA is defined to a large extent by the relative orientation of its helical domains which are generally linked by functionally important internal loops, bulges, and other junctions. Many processes including ribozyme catalysis, ribonucleoprotein assembly, and RNA-ligand recognition feature large changes in the orientation of helical domains that allow one RNA structure to adaptively satisfy multiple structural requirements (Leulliot and Varani, 2001; Lilley, 2004; Al-Hashimi, 2005). Thus, the relative orientation and dynamics of helical domains is a key feature of RNA folding, structure, and function.

Residual dipolar couplings (rdcs) (Tolman et al., 1995; Tjandra and Bax, 1997; Prestegard

*To whom correspondence should be addressed. E-mail: hashimi@umich.edu

et al., 2000) are particularly well suited for determining the relative orientation and dynamics of molecular fragments (Losonczi et al., 1999; Mollova et al., 2000; Trantirek et al., 2000; Sibille et al., 2001; Tolman et al., 2001; Al-Hashimi et al., 2002a, b). The key to these approaches is the determination of order tensors that describe partial alignment relative to the applied magnetic field (Saupe, 1968; Tjandra and Bax, 1997; Losonczi et al., 1999; Trantirek et al., 2000; Tolman et al., 2001; Zweckstetter, 2003). This in turn requires the measurement of five or more independent rdcs per fragment and knowledge regarding the fragment's local structure and specifically the relative orientation of the rdc targeted vectors. In nucleic acids, strategies have been developed that combine rdcs with other experimental and non-experimental restraints in the simultaneous *de novo* determination of the local structure of fragments and their order tensors (Sibille et al., 2001; McCallum and Pardi, 2003). Alternatively, the idealized A-form helix has been used to model Watson–Crick helical segments (Mollova et al., 2000; Al-Hashimi et al., 2002b). Since this obviates the need to solve the local helix structure, it makes possible a number of unique applications. For example, it may allow the relative orientation and dynamics of helical domains to be characterized for RNAs deemed too large for complete high-resolution structure determination. The demonstrated high efficiency of these rdc approaches also makes possible systematic studies of how RNA's global conformational dynamics varies in response to changes in environmental conditions (Al-Hashimi et al., 2002a, 2003; Pitt et al., 2004, 2005; Reiter et al., 2004). The problem, however, is that static and/or dynamic deviations from the assumed idealized A-form geometry will lead to order tensor errors (Zweckstetter and Bax, 2002) that can misguide interpretation in terms of RNA global structural dynamics.

In this study, we examined both theoretically and experimentally how static and dynamic deviations from the idealized A-form geometry together with rdc measurement uncertainty impact order tensors derived using rdcs. Our results show that provided a sufficient number of rdc measurements (≥11), order tensors can be determined at a useful level of accuracy and precision.

Materials and methods

Molecular dynamics (MD) simulation of solvated HIV-1 TAR RNA

A 20-ns MD simulation of wild-type TAR was performed using the CHARMM force field with the parameter set 27 (MacKerell et al., 2000). Starting coordinates were obtained from structure 3 of the family of free TAR NMR structures (PDB 1ANR) (Aboul-ela et al., 1996). This structure was chosen as it yields the best agreement with previously measured rdcs (Al-Hashimi et al., 2002b). The RNA was neutralized using sodium counter ions and solvated in a 35 Å sphere of TIP3P water (Jorgensen et al., 1983) and a stochastic boundary potential was used (Brooks and Karplus, 1983); this setup allowed for >9 Å distance between the surface of the sphere and all RNA atoms. This system was minimized and heated to 300 K while harmonically constraining the heavy atoms of the RNA with a force constant of 62 kcal/mol/A^2 for 100 ps, after which the constraints were removed. A Nóse–Hoover thermostat (Nose, 1984; Hoover, 1985) was used to maintain a constant temperature of 300 K throughout the simulation, with a 1 fs time step and a coupling constant of 50 ps^{-1}. Lipari–Szabo spin relaxation order parameters (S^2) (Lipari and Szabo, 1982) were calculated for base and sugar vectors. The value of S^2 was computed from the tail (averaged over the last 500 time steps) of the calculated P_2 auto-correlation function ($C(t) = \frac{3(\mu(0)\cdot\mu(t))^2-1}{2}$, where μ is the bond vector position in Cartesian space) describing the dynamics of each bond vector (Lipari and Szabo, 1982; Bruschweiler, 2003). In order to take into account only local motions of the bond vector relative to the overall A-form helix, correlation functions were calculated separately for each helix using the heavy atoms of each helix as the reference for overlaying trajectory snapshots.

Statistical survey of free and ligand-bound A-form RNA structures and implementation of A-form angular deviations

We used the search tools in the nucleic acid database (NDB) (http://ndbserver.rutgers.edu) (Berman et al., 1992) to perform a statistical survey of A-form helices in a variety of RNA structural

contexts. Specifically, we conducted a search over X-ray structures of RNA that have been solved with < 3 Å resolution using the 'A-form' option under 'structural features' imposing no other restrictions in the search. The same search was repeated for RNA structures that contain ligands using the 'ligand' option under 'biomolecules contain'. This yielded a total of 20 unbound RNA structures comprising 104 base-pairs (AR0001, AR0002, AR0005, AR0008, AR0011, AR0022, AR0027, AR0032, AR0039, AR0064, ARH063, ARH074, ARH064, ARL037, ARL048, ARL062, ARN035, URL029, URX063, ARF0108) and 20 ligand-bound RNA structures comprising 128 base-pairs (AR0006, AR0009, AR0010, AR0012, AR0013, AR0026, AR0028, AR0030, AR0056, AR0061, AR0065, DR0006, DR0011, DR0015, DR0016, DR0017, DR0019, DR0020, DR0021, DR0022). Within each of these structures, only non-terminal Watson–Crick base-pairs (GC, CG, AU, UA) that are flanked on either side by at least one other WC base-pair were analyzed. Including terminal residues had a negligible impact on statistics for base-pair parameters in the unbound structures, but did have an impact on the base-pair step parameters in the unbound structures and both base-pair and base-pair step parameters in the ligand-bound structures. The base-pair and base-pair step angles buckle (κ), propeller (ω), opening (σ), incline (η), tip (θ), and twist (Ω) were computed using the NDB web-server which employs the program 3DNA (Lu and Olson, 2003). The sugar torsions ($\nu_0 - \nu_4$) were obtained for the same nucleotides using the program PROSIT (Sun et al., 2004). The distributions of angles for unbound and ligand-bound RNA structures were independently fitted to a Gaussian distribution using the program Origin7.0 (OriginLab Corp). The computed mean angles and standard deviations are listed in Table 1.

To implement these A-form angular deviations, the six base-pair angles (κ, ω, σ, θ, η, and Ω) were consolidated into three effective angles that can be conveniently varied via rotations around the *x*-, *y*-, and *z*-axes of the standard reference frame (Figure 3a). These angles include base incline ($\eta_L = (2\eta + \kappa)/2,\ \eta_R = (\eta_L - \kappa)$) (rotation around the *x*-axis) and tip ($\theta_L = (2\theta + \omega)/2,\ \theta_R = (\omega - \theta_L)$) (rotation around the *y*-axis), and helical twist (Ω) (rotation around the *z*-axis) (see Figure 3c). Tip and incline were averaged over the 'left' and 'right' bases to obtain one value for each parameter, η_B and θ_B. In implementing A-form deviations, each base received a random combination of rotations around the *x*-, *y*- and *z*-axes with amplitudes that follow the Gaussian standard deviations in Table 1 (see

Table 1. Mean angles and standard deviations (shown in parenthesis) for base and sugar angles obtained in this study for unbound (Unbound RNA A-form) and ligand-bound (Ligand-bound RNA A-form) A-form RNA helices using a statistical survey of X-ray structures solved with < 3.0 Å resolution. Also shown are the mean and standard deviations for base angles previously reported for the idealized RNA (Neidle, 1999) and DNA (Olson et al., 2001) A-form helices respectively. The mean and standard deviations for the sugar torsion angles ($\nu_0 - \nu_4$) shown under 'Idealized RNA A-form' were obtained from a previous survey of X-ray structures of nucleotides (Gelbin et al., 1996).

	Unbound RNA A-form (20 structures)	Ligand-bound RNA A-form (20 structures)	Idealized RNA A-form	Idealized DNA A-form
Buckle (κ)	0.3 (6.8)	0.4 (4.8)	0	− 0.1 (7.8)
Propeller Twist (ω)	− 12.5 (7.3)	− 12.2 (4.7)	− 14.5	− 11.8 (4.1)
Opening (σ)	0.3 (3.9)	1.6 (3.2)	4.2	0.6 (2.8)
Incline (η)	16.0 (8.7)	14.9 (8.0)	15.8	14.7 (7.3)
Tip (θ)	− 0.5 (6.9)	− 0.7 (4.9)	0	− 0.1 (5.2)
Twist (Ω)	33.2 (3.8)	32.6 (3.9)	32.7	32.5 (3.8)
Base Incline (η_B)	15.9 (9.4)	13.7 (8.5)		
Base Tip (θ_B)	− 6.3 (7.9)	− 6.0 (5.6)		
ν_0	2.0 (5.9)	2.1 (4.2)	2.8 (6.1)	
ν_1	− 26.8 (4.9)	− 27.0 (3.3)	− 24.6 (4.9)	
ν_2	40.3 (4.2)	40.3 (2.7)	35.9 (2.8)	
ν_3	− 40.2 (4.6)	− 40.3 (3.2)	− 32.3 (3.1)	
ν_4	24.0 (5.8)	23.9 (4.1)	20.5 (5.1)	

unbound RNA A-form). Variations in sugar torsion angles were approximated by rotation of each C–H bond about its opposite vector in the ring, as shown for example by a dashed line for the C2′–H2′ vector in Figure 3b. Standard deviations corresponding to the largest torsion angle involving the carbon were used (i.e. C1′/C3′ = 5.8° and C2′/C4′ = 5.9°) (Table 1).

Simulations for determining order tensor error due to rdc uncertainty and A-form angular deviations

Numerical simulations for evaluating the order tensor error due to angular deviations and rdc uncertainty were performed using in-house programs. The domain I A-form helix of HIV-1 TAR (see Figure 1a) was used for all simulations. Idealized A-form helices were constructed using Insight II (Molecular Simulations, Inc). Importantly, the RNA A-form helices generated by Insight II 2000.1 have an incorrect sign for propeller twist angles (+15°). Thus, the propeller twist angles were corrected via rotation around the *y*-axis of the standard reference frame to be −15° (Neidle, 1999). A-form angular noise was added as described above to generate a ''real'' helix. One bond C–H rdcs were then computed for the ''real'' helix assuming an order tensor with $S_{zz} = 0.001$, $\eta = |(S_{yy} - S_{xx})|/S_{zz} = 0.20$, and principal axis ($S_{zz}$) oriented 35° off from the helix axis. Simulations were also repeated with S_{zz} oriented parallel to and 70° and 90° off from the helix axis as well as with varying asymmetry parameters (η) (Supplementary material, Figure S1).

Different rdc sets were tested comprising commonly measured one bond C–H rdcs in base ($^1D_{C2H2}$, $^1D_{C5H5}$, $^1D_{C6H6}$, $^1D_{C8H8}$) and sugar ($^1D_{C1'H1'}$, $^1D_{C2'H2'}$, $^1D_{C3'H3'}$, and $^1D_{C4'H4'}$) moieties. Specifically four rdc sets were used, comprising 8, 11, 17 and 29 rdcs, respectively that yield a bond vector distribution defined by condition numbers (CN) (Tolman et al., 2001) of 4.5, 2.5, 2.5, and 2.3, respectively (Supplementary material, Table S1). The data sets were modeled after experimental sets previously measured in helix I of TAR (Al-Hashimi et al., 2002b). All sets were a subset of the 29 rdc set which comprised 6 C8H8, 2 C6H6, 4 C5H5, 1 C2H2, 2 C4′H4′, 2 C3′H3′, 5 C2′H2′, and 7 C1′H1′ vectors across the 6 base-pairs of helix I in HIV-1 TAR (Supplementary material, Table S1). The sets span a different number of base-pairs (2, 2, 4 and 6, respectively), however similar results were obtained when increasing the number of rdcs without increasing

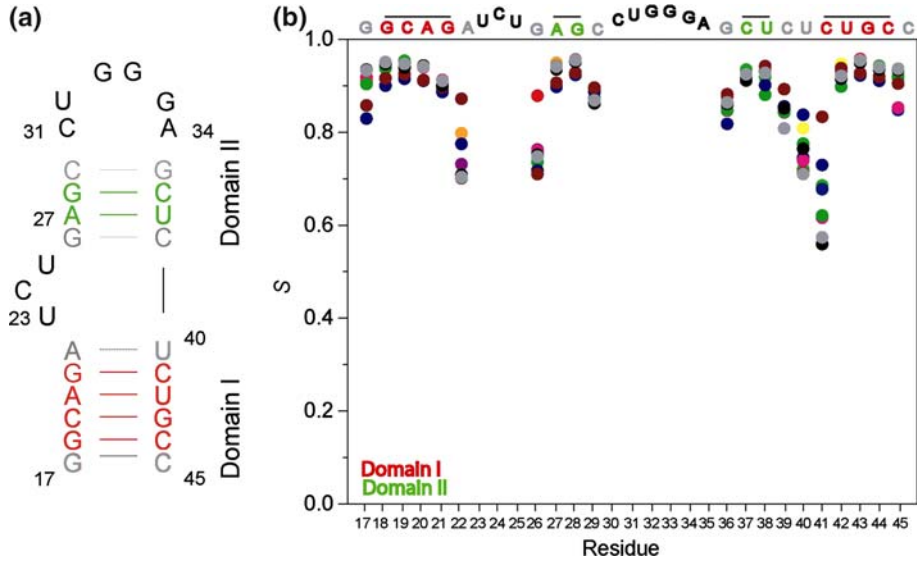

Figure 1. (a) Secondary structure of wild-type HIV-1 TAR. Helix terminal base-pairs are shown in gray. (b) The square root of the Lipari–Szabo order parameter (*S*) for C–H and N–H bonds in wild-type HIV-1 TAR RNA as a function of residue computed from a 20-ns MD simulation in explicit solvent. Values for base N1H1, C2H2, N3H3, C5H5, C6H6, C8H8 and sugar C1′H1′, C2′H2′, C3′H3′, C4′H4′, C5′H5′, C5′H5″ bonds are shown in red, orange, yellow, green, blue, purple pink, olive, indigo, brown, black, and gray, respectively.

the total number of base-pairs (Supplementary material, Figure S2). For a given number of rdcs, similar results were also obtained when changing the identity of the input C–H rdcs but maintaining a mixture of sugar and base rdcs such that CN < 5 (data not shown). Depending on the simulation, Gaussian uncertainty of 1.5 Hz was introduced to the computed rdcs. The idealized A-form helix and rdcs were then used to compute best-fit order tensors using a modified version of the program ORDERTEN_SVD (Losonczi et al., 1999). A given simulation was repeated 1000 times each time sampling a different "real" A-form structure and rdc uncertainty. The order tensor error was then deduced by computing the root-mean-square-deviation (rmsd) in the generalized degree of order $\left(\mathrm{GDO} = \sqrt{2/3(S_{xx}^2 + S_{yy}^2 + S_{zz}^2)}\right)$ and principal S_{zz} (ΔS_{zz}) orientation:

$$\mathrm{rmsd(GDO)} = \frac{1}{\mathrm{GDO_{true}}} \sqrt{\frac{\sum_N (\mathrm{GDO_{true}} - \mathrm{GDO_{calc}})^2}{N}}$$

$$\text{and } \mathrm{rmsd}(S_{zz}) = \sqrt{\frac{\sum_N (\Delta S_{zz})^2}{N}} \qquad (1)$$

where N is the total number of measured rdcs.

The S_{zz} orientation and GDO play the dominant role defining the inter-helical angle and dynamics, respectively, thus we do not present an error analysis of the individual S_{xx} and S_{yy} axes of order.

The computed order tensor and idealized A-form helix were also used to back-predict rdcs and the rmsd between the measured and back-predicted rdcs evaluated:

$$\mathrm{rmsd(rdc{:}aform)} = \sqrt{\frac{\sum_N \left(\mathrm{rdc_{exp}} - \mathrm{rdc_{calc}}\right)^2}{N}}. \qquad (2)$$

Estimating errors in order tensors determined for A-form helices using 'Aform-RDC'

Separate simulations employing the same four rdc sets were used to validate a protocol for estimating the errors in order tensors determined for A-form helices using experimental rdcs ('Aform-RDC'). In Aform-RDC, simulations analogous to those used for examining the impact of angular noise and rdc error are performed on an experimental rdc vector set. Starting order tensor parameters for the simulations are obtained from best-fitting the input rdc data to the idealized A-form helix. Simulations are then conducted using the vector set corresponding to the measured rdcs, with the rdc uncertainty set equal to that estimated experimentally. The magnitude of A-form angular noise is initially set to a value $L_{\mathrm{trial}} = 0.1$, which corresponds to a scaling ($0.1x$) of the implemented angular standard deviations (Table 1, unbound RNA A-form η_B, θ_B, and Ω). The value of L_{trial} is increased in increments of 0.1 to a final value of, L_{exp}, that yields a mean rmsd(rdc) (over 1000 runs) that is comparable to that observed experimentally when fitting rdcs to the idealized A-form geometry (rmsd(rdc:aform)). The uncertainty in the GDO and S_{zz} orientation obtained in the simulations with the scaling factor $L = L_{\mathrm{exp}}$ are estimated to be the experimental uncertainty in these parameters. Aform-RDC was validated using a set of 100 theoretical structures each having different combinations of angular noise with $L = 1.0$ and rdc error of 1.5 Hz with a starting value of $S_{zz} = 0.001$, $\eta = 0.2$, and S_{zz} oriented at 35° to the helix axis. Simulations were also repeated with S_{zz} oriented parallel to and 70° and 90° off from the helix axis as well as with varying asymmetry parameters (η) (Supplementary material, Figure S3).

Aform-RDC was used to analyze experimental rdcs measured in the two TAR helices in the free form (Al-Hashimi et al., 2002b) and when bound to Mg^{2+} (Al-Hashimi et al., 2003), argininamide (Arg) (Pitt et al., 2004), the aminoglycoside neomycin B (NeoB) (Pitt et al., 2005), and the small molecule acetylpromazine (Acp) (Pitt et al., 2005). Rdcs from base-pairs at helix termini were excluded except for the closing C29-G36 base-pair below the stabilizing UUCG loop which has been shown to be locally stable (Duchardt and Schwalbe, 2005; Vallurupalli and Kay, 2005). Input/output parameters related to this Aform-RDC analysis are summarized in Table 2. All bond lengths (r) used in these calculations were derived from the AMBER force field (Cornell et al., 1995).

Table 2. Aform-RDC analysis of rdcs measured in two TAR helices (I and II) in the free state (TAR-Free) and bound to four different ligands (Acp, Arg, Mg^{2+}(3.0:1) and NeoB)

	TAR-Free		TAR-Acp		TAR-Arg		TAR-Mg (3:1)		TAR-NeoB	
	I	II	I	II	I	II	I	II	I	II
N	16	11	18	13	17	15	10	10	16	13
σ(rdc) (Hz)	1.1	1.1	2.0	2.0	1.9	1.9	2.5	2.5	2.2	2.2
L_{exp}	0.8	0.6	1.2	0.5	0.4	0.2	0.7	1.6	1.2	0.6
A-form GDO ($\times 10^{-3}$)	0.48 (3.8%)	0.88 (3.5%)	1.09 (4.1%)	1.70 (3.1%)	1.37 (1.7%)	1.52 (1.4%)	1.03 (7.2%)	1.11 (7.7%)	1.42 (4.9%)	1.42 (5.7%)
A-form rmsd (S_{zz}) (°)	4	2	6	2	2	1	6	4	6	4
A-form GDO_{int}	0.56 (5.2%)		0.64 (5.1%)		0.90 (2.2%)		0.97 (10.5%)		0.99 (7.5%)	
	0.59		*0.69*		*0.93*		*0.93*		*0.94*	
A-form Inter-helical	46 (4)		48 (6)		14 (2)		7 (7)		30 (7)	
Angle (°)	*46*		*43*		*11*		*12*		*18*	

In all cases, rdcs were measured in a TAR construct in which the wild-type loop was replaced with a UUCG loop. Shown for each helical domain is the number of rdcs (*N*), previously reported rdc uncertainty (σ(rdc)), the angular deviation scaling factor (L_{exp}), the GDO when fitting rdcs to A-form helices (A-form GDO) with errors estimated using Aform-RDC, the Aform-RDC estimated error in the S_{zz} orientation, the GDO_{int} (GDO(I)/GDO(II)) values when fitting the rdcs to a proper A-form structure (A-form GDO_{int}) together with the Aform-RDC estimated errors, and the inter-helical angles for the A-form structures (A-form Inter-helical Angle) with errors estimated from the Aform-RDC S_{zz} orientation errors. (Note that the errors in the inter-helical angles are likely underestimated as this value does not account for errors in the S_{xx} and S_{yy} orientations). Corresponding values reported previously when fitting rdcs to an A-form structure with the incorrect propeller twist are shown in italics.

Results

Dynamic deviations from the A-form helix

Local motions occurring at sub-millisecond timescales will lead to motional averaging of measured rdcs (Tolman et al., 1997). Heterogeneity in dynamics across different bond vectors or helical domains leading to different degrees of motional averaging will result in a set of rdcs that cannot rigorously be accounted for on the basis of a single order tensor. As a result, fitting of such rdcs to a single idealized structure will lead to order tensor errors.

Thus far, the effects of local motional averaging have largely been ignored in rdc studies of nucleic acids. This might be justified for central Watson–Crick base-pairs where local motions are expected to be similar in amplitude. If one further assumes that these motions are spatially isotropic, then their effect will be to simply uniformly scale down measured rdcs and derived order tensor elements by S, where S^2 is the Lipari–Szabo spin relaxation order parameter (Lipari and Szabo, 1982; Tolman et al., 1997). This would not adversely affect analyses that compare helix-specific order tensors.

To examine the validity of this assumption, we surveyed recent NMR relaxation studies of RNA dynamics focusing on non-terminal hydrogen bonded Watson–Crick residues in A-form helices (Duchardt and Schwalbe, 2005; Shajani and Varani, 2005; Showalter et al., 2005; Vallurupalli and Kay, 2005; Zhang et al., 2006). Of note is a recent ^{2}H relaxation study that allowed quantitative measurements of dynamics in a prototypical stem-loop RNA without some of the complications associated with the interpretation of ^{13}C relaxation data. Very similar S values were reported across different base and sugar vectors in non-terminal Watson–Crick base-pairs (mean values and ranges are 0.93 (0.90–0.95), 0.94 (0.93–0.95), 0.91 (0.91–0.94), 0.94 (0.94–0.94), and 0.94 (0.94–0.95) for D1′, D2′, D4′, D5, and D6, respectively) (Vallurupalli and Kay, 2005). Similar S values have been independently reported for a different bulge containing RNA for imino N1H1 (0.92 (0.91–0.93)) and N3H3 (0.91 (0.89–0.93)) by ^{15}N relaxation measurements (Zhang et al., 2006). Equally small variations in S have also been reported by ^{13}C relaxation measurements (Duchardt and Schwalbe, 2005; Shajani and Varani, 2005; Showalter et al., 2005).

To further examine the amplitude of local motions over an expanded set of inter-nuclear vectors and over slightly longer timescales, we ran a 20-ns MD simulation of solvated wild-type HIV-1 TAR RNA (Figure 1a). Analysis of time correlation functions computed from the MD trajectory allowed calculation of S for any internuclear bond vector (see Materials and methods). With the exception of C41, for which the correlation functions had not yet converged, very similar S values were computed for various rdc vectors across different non-terminal residues in the two helices (Figure 1b), which are also in excellent agreement with counterparts reported in the ^{2}H and ^{15}N relaxation studies. Mean values and ranges are 0.94 (0.91–0.96), 0.94 (0.94–0.95), 0.94 (0.94–0.95), 0.93 (0.93–0.94), 0.93 (0.92–0.95), 0.95 (0.94–0.95), 0.94 (0.89–0.95), 0.93 (0.88–0.95), 0.91 (0.89–0.92), 0.92 (0.90–0.94), 0.93 (0.90–0.95), and 0.93 (0.91–0.96) for N1H1, N3H3, C8H8, C6H6, C5H5, C2H2, C1′H1′, C2′H2′, C3′H3′, C4′H4′, C5′H5′, and C5′H5″, respectively. Smaller S values are observed for terminal base-pairs A22-U40 and G26-C39 indicating that their rdcs are more susceptible to motional averaging. Rdcs from such terminal base-pairs are therefore best excluded in the determination of order tensors for A-form helices.

The above analysis strongly suggests that local motions in non-terminal Watson–Crick base-pairs will uniformly scale down rdcs and derived order tensor elements by $\sim$7%. This will not adversely affect the determination of RNA's global conformational dynamics based on comparison of helix-specific order tensors. However, this uniform scaling should be taken into account in interpreting field-induced rdcs in terms of the sum of magnetic susceptibility tensors of individual nucleobases (Zhang et al., 2003; Bryce et al., 2004; van Buuren et al., 2004).

Static deviations from the idealized A-form helix obtained from statistical comparison of RNA X-ray structures

Static deviations in the angular orientation of rdc vectors from the assumed idealized A-form geometry will lead to order tensor errors. The geometry of a given nucleotide is described by six backbone torsion angles (α, β, δ, ε, γ, and ζ), five sugar torsion angles ($\nu_0 - \nu_4$), and the glycosidic bond (χ). Parameters have also been developed

that describe base and base-pair orientations within a helix; buckle (κ), propeller twist (ω), and opening (σ) describe the relative orientation of bases within a base-pair whereas tilt (τ), roll (ρ), and twist (Ω) describe the orientation of base-pairs relative to each other, and finally tip (θ) and inclination (η) describe the orientation of base-pairs relative to a local or global axis (Dickerson, 1988). To obtain insight into static deviations from the idealized A-form helix, and indeed to validate the current idealized A-form helix geometry, we performed a statistical survey of 232 non-terminal Watson–Crick bases in a total of 20 unbound and 20 ligand-bound RNA X-ray structures respectively derived from the Nucleic Acid Database (NDB) (Berman et al., 1992) that have been solved with < 3.0 Å resolution. The results of these calculations are summarized in Table 1 and distributions for unbound RNA shown in Figure 2. In all cases, the distribution of angles was nearly Gaussian ($R^2 = 0.88$–0.99), allowing parameterization in terms of a single mean and standard deviation (Table 1).

Very similar mean/standard deviations were obtained for unbound and ligand-bound RNA structures (Table 1). In fact, the standard deviations for both sugar torsion and base angles were slightly lower for the ligand-bound structures. The mean angles defining the orientation of bases are in excellent agreement with the widely accepted idealized RNA helix (Neidle, 1999) (Table 1). The most notable exception is our opening angle (~0°) which is in better agreement with that reported for the DNA (~0°) (Olson et al., 2001) compared to RNA (4.2°) (Neidle, 1999) A-form helix. As shown in Table 1, the standard deviations we obtain for the A-form RNA helix are very similar to those reported previously for the A-form

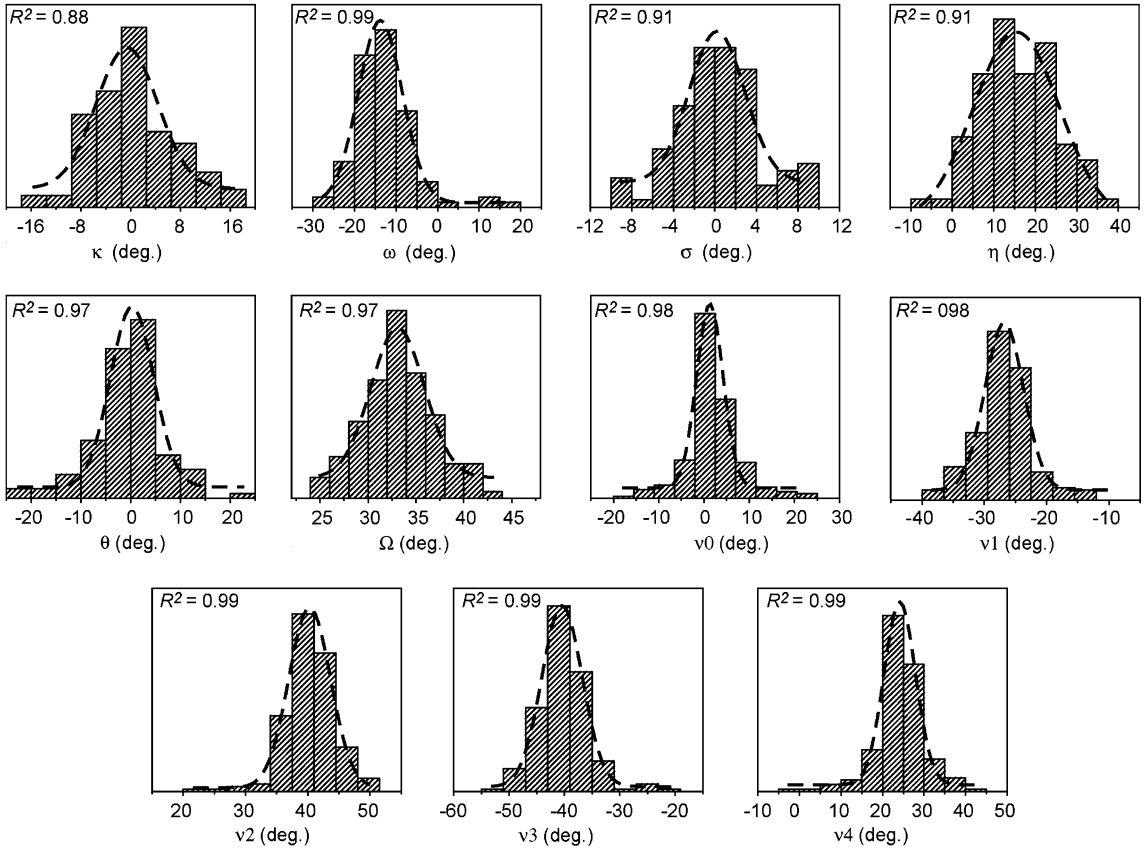

Figure 2. Angular distribution for buckle (κ), propeller twist (ω), opening (σ), incline (η), tip (θ), twist (Ω), and sugar ring torsion ($\nu_0 - \nu_4$) angles. Best-fit Gaussian distributions are shown using dashed curves together with the corresponding correlation coefficient (R^2). These distributions were obtained from a statistical survey of X-ray structures for unbound RNAs solved with < 3.0 Å resolution.

DNA helix (Olson et al., 2001), with the deviations in propeller twist, opening, incline, and tip angles being on average slightly larger (~1.7°) for RNA. The mean and standard deviations obtained for the sugar ring torsion angles are in very good agreement with counterparts reported previously based on a statistical survey of nucleotide X-ray structures (Gelbin et al., 1996), with the largest differences observed for ν_2 and ν_3 for which our mean values were ~4° and ~8° larger, respectively.

For both unbound and bound RNA structures, the largest standard deviations are observed for buckle, incline, propeller twist, and tip angles (Table 1). For the unbound RNA structures, these are 6.8°, 8.7°, 7.3°, and 6.9°, respectively. These four deviations can be combined into net deviations in base incline (9.4°) and tip (7.9°) angles (Table 1). The latter correspond to rotations of bases around the *x*- and *y*-axes respectively of the standard reference frame (Figure 3a). Since these deviations will on average lead to the largest

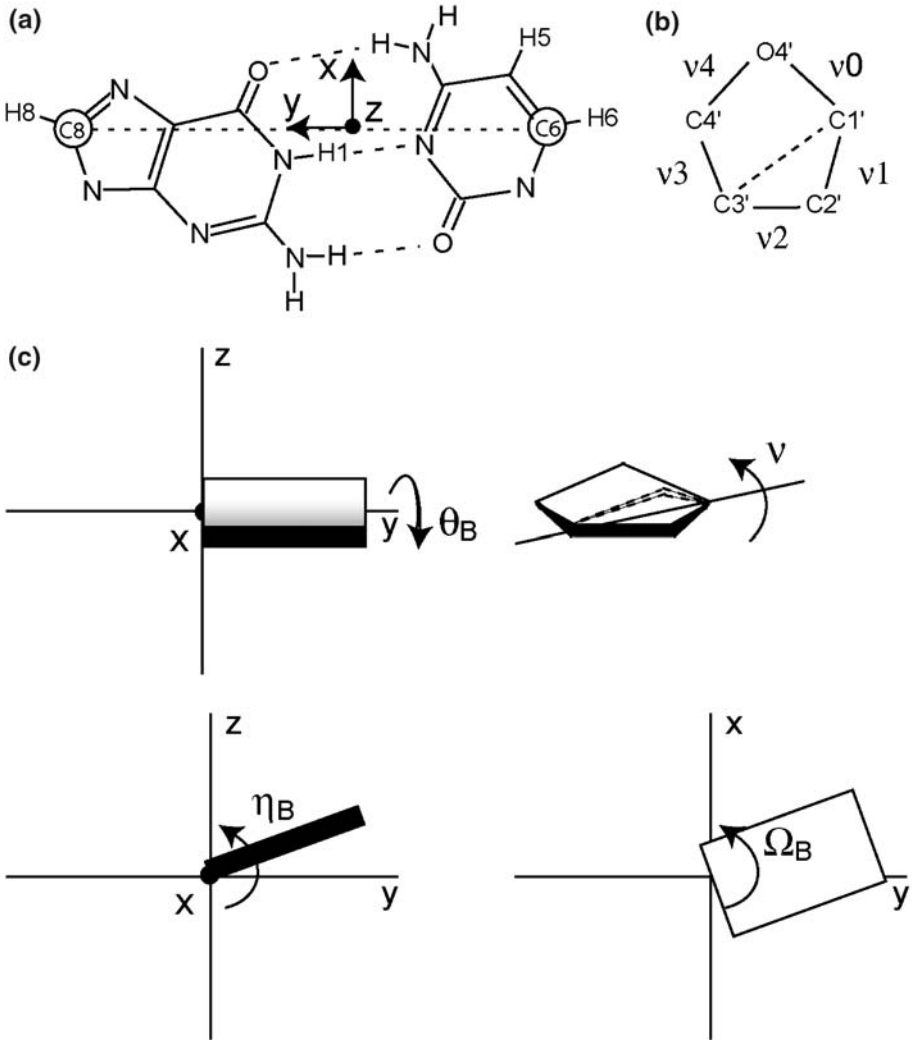

Figure 3. Implementation of base and sugar A-form angular deviations. (a) The standard base-pair reference frame (Olson et al., 2001) in which the *y*-axis runs from the purine C8 to the pyrimidine C6 and the *z*-axis is oriented along the mean of the base normals. (b) The sugar torsion angles ($\nu_0 - \nu_4$). Reorientation of sugar C–H vectors due to variations in sugar torsion angles are approximated by single axis rotations of the C–H vector around its opposite vector in the ring, shown as a dashed line for C2′–H2′. (c) Depiction of the single axis rotations that were applied to the bases (η_B, θ_B, and Ω_B) and sugar rings (ν) used to generate A-form angular deviations.

changes in the orientation of rdc vectors relative to the principal axis of order (S_{zz}), they are also expected to dominate order tensor errors due to angular deviations in the bases. In contrast, the deviations are smaller for the opening (3.9°) and twist (3.8°) angles which will generally be less effective in changing the orientation of rdc vectors relative to S_{zz} and thus less capable of inducing order tensor errors. The deviations in sugar torsion angles can be characterized as moderate all being $<6.0°$ (Table 1). Overall, the observed angular deviations do not make certain rdc vectors significantly less susceptible to angular noise than others.

The structures surveyed here represent helical elements under diverse crystallization conditions within relatively small RNA elements that exemplify RNA fragments studied by NMR. However, very similar distributions of angular parameters were obtained when including 189 additional base-pairs from the ribosome structure (PDB 1JJ2, Klein et al., 2001) (Supplementary material, Table S2).

Impact of static A-form angular deviations and rdc uncertainty on derived order tensors

We used computer simulations (see Materials and methods) to examine the order tensor errors arising due to the Gaussian A-form angular deviations as determined from a statistical survey (unbound RNA A-form, Table 1) and typical Gaussian rdc measurement error (1.5 Hz at 10^{-3} level of order) (Mollova et al., 2000; Warren and Moore, 2001; Al-Hashimi et al., 2002b; Bondensgaard et al., 2002; McCallum and Pardi, 2003; Pitt et al., 2004, 2005). Shown in Figure 4 is the error in the generalized degree of order (rmsd(GDO)) (Tolman et al., 2001) (Figure 4a) and orientation of the principal S_{zz} direction (rmsd(S_{zz})) (Figure 4b) arising due to rdc error (open), A-form angular deviations (dashed), and a combination of rdc error and angular deviations (filled). Results are shown for 8, 11, 17, and 29 one bond base and sugar C–H rdcs that reflect an rdc distribution previously obtained for helix I of TAR (Al-Hashimi et al., 2002b). Results are shown assuming a real order tensor with $S_{zz} = 0.001$, $\eta = |(S_{yy} - S_{xx})/S_{zz}| = 0.20$, and the principal axis (S_{zz}) oriented 35° away from the helix axis. Simulations were also performed with S_{zz} orientated parallel to, and at 70° and 90° relative

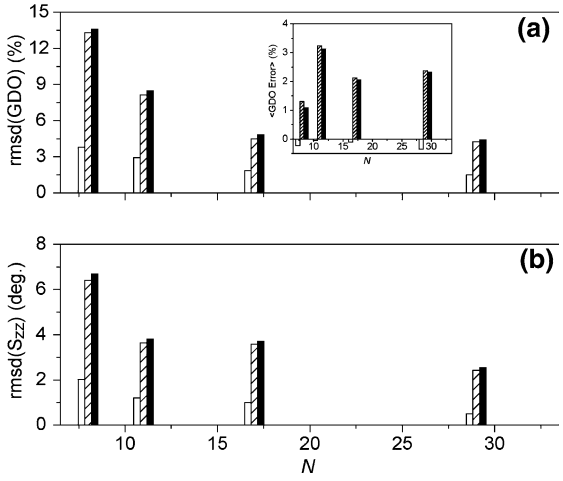

Figure 4. Order tensor errors induced by 1.5 Hz rdc error (open), A-form angular deviations (dashed), and a combination of 1.5 Hz rdc error and A-form angular deviations (filled) for 8, 11, 17, and 29 sugar and base C–H rdcs and a starting order tensor of $S_{zz} = 0.001$ and $\eta = 0.20$. Shown are the errors in (a) GDO (rmsd(GDO), defined in Equation (1)) and (b) S_{zz} orientation (rmsd(S_{zz}), defined in Equation(1)). Results are shown over 1000 runs each sampling different rdc error and/or angular deviations. Shown in the inset is the average GDO error $\left(\frac{|\mathrm{GDO_{true}} - \mathrm{GDO_{calc}}|}{\mathrm{GDO_{true}}} \cdot 100\right)$ as a function of the number of rdcs. No internal motions were assumed.

to the helix axis (Supplementary material, Figure S1(a, b)), showing a slight variance of the errors depending on the orientation of the helix. Very small differences were also observed in simulations with different asymmetries (η) (Supplementary material, Figure S1(c, d)). The overall trends in the order tensor errors are similar to those reported previously in a study examining order tensor errors in hypothetical structures due to random structural noise (Zweckstetter and Bax, 2002). The errors in the GDO and S_{zz} orientation increase monotonically with decreasing number of rdcs (N) with disproportionately larger errors observed for $N \leq 7$ as the system of equations becomes underdetermined (data not shown). While the rdc uncertainty results in random GDO errors, angular noise leads to its systematic underestimation which varies as a function of the number of rdcs (Figure 4a, inset). The underestimation increases with increasing rdcs for $N \leq 11$, but for $N > 11$ the underestimation plateaus to a value of ~2%. A similar trend was observed in the previous study of hypothetical structures employing random structural noise (see Zweckstetter and Bax, 2002,

Figure 5). In contrast, the S_{zz} orientation error was always randomly distributed (mean deviation ≤1.5°, data not shown).

For all four rdc sets examined, rdc error led to on average < 4% error in the GDO and < 2° deviations in the orientation of S_{zz}. In contrast, angular deviations alone led to < 14% and < 7° error in the GDO and S_{zz} orientation, respectively. The combined order tensor error is roughly equal to the square root of the sum of the squares of each error contribution (< 14% and < 7°, respectively). Thus, the order tensor error is dominated by angular deviations. Interestingly, even for the less ideal case of 11 rdcs, the net error in the GDO and S_{zz} orientation (Figure 4) remains on average sufficiently small (< 9% and < 4°, respectively) to allow useful inferences to be made regarding the relative orientation and dynamics of RNA helices. However, it should be noted that these results are for rdc sets with a relatively good distribution of base and sugar RDCs (CN< 5) and that significantly larger errors are observed when the bond vector distribution is less ideal (i.e. CN > 8). For the more favorable case of having ≥17 rdcs, the average errors are < 5% and < 4°, respectively with similar errors (< 5% and < 3°) observed for 29 rdcs. The reduction in the order tensor error with increasing number of rdcs was independent of whether the rdcs spanned two, four, or six base-pairs (Supplementary material, Figure S2). Thus, increasing the rdcs measured can allow accurate determination of order tensors for smaller and smaller A-form fragments (Boisbouvier et al., 2004; O'Neil-Cabello et al., 2004; Jaroniec et al., 2005). Additionally, we note that the errors shown in Figure 4 are averages and that the error for any given case can be smaller or larger. For example, for 17 rdcs the error in the GDO and S_{zz} orientation were as large 17% and 12°, respectively. Finally, we note that despite the reduced sampling of structural noise, similar results were obtained when using the actual crystal structures included in our NDB survey as the noise corrupted structures. For example, for 17 rdcs, the GDO and S_{zz} orientation rmsds were 7.1% and 8.8°, respectively.

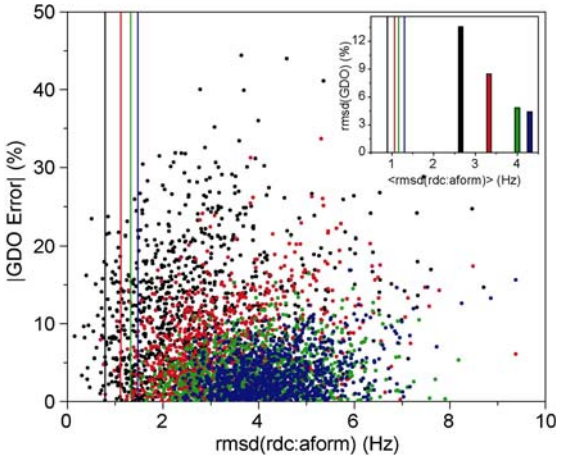

Figure 5. Correlation between the error in the GDO and the rdc rmsd value (rmsd(rdc:aform), see Equation (2)) for 1000 individual runs in the presence of angular deviations and 1.5 Hz rdc error. Results are shown for 8 (black), 11 (red), 17 (green), and 29 (blue) rdcs with a starting order tensor of $S_{zz} = 0.001$ and $\eta = 0.20$. Shown in the inset is the rmsd(GDO) over the 1000 runs for each set of vectors as a function of the average rmsd(rdc:aform). Vertical lines show the average rmsd for only 1.5 Hz rdc error for each set.

Estimating errors in order tensors determined for A-form helices (Aform-RDC)

Given the magnitude of order tensor error that can result from angular noise, use of the idealized A-form helix in rdc applications requires robust methods for assessing its validity and perhaps more importantly for evaluating the net error in the order tensor arising due to the combined effects of angular noise and rdc measurement uncertainty. As shown in Figure 5, there exists a correlation between the net GDO error and the rmsd between measured rdcs and values back-predicted using the best-fitted order tensor and the idealized A-form helix (rmsd(rdc:aform)) (similar correlation is observed for the S_{zz} orientation, data not shown). The correlation improves with increasing number of rdcs (Figure 5), noting that for ≥17 rdcs, the error for order tensors yielding rmsd(rdc:aform) approaching values expected from rdc error only is negligible. The correlation also varies depending on the specific choice of rdc vectors and the orientation of rdc vectors relative to the order tensor PAS. Additionally, the value of rmsd(rdc:aform) depends on the degree of alignment which modulates the relative contributions from rdc uncertainty and angular deviations. Thus, although the value of rmsd(rdc:aform) can be used to gauge the net order tensor error, any such implementation will have to take into account the particularities of the rdc data set in hand.

To this, end we have implemented a simple and robust approach that can be tailored to specific experimental situations which uses the value of rmsd(rdc:aform) to estimate the net order tensor error (see Materials and methods). Here, simulations analogous to those used to estimate order tensor errors due to rdc uncertainty and angular noise are performed, where the 'real' order tensor corresponds to that obtained from best-fitting the experimental rdcs to the idealized A-form helix and the rdc vectors and their uncertainty correspond to that measured experimentally. Simulations are then performed as a function of increasing angular deviations until a level is reached (L_{exp}) that yields an average rmsd(rdc:aform) equal to that obtained experimentally. The resulting order tensor errors are then used as estimates for the real experimental order tensor error. A similar approach was previously proposed for the case of hypothetical structures with random structural noise (Zweckstetter and Bax, 2002). In this ''structural noise Monte-Carlo method'' random structural noise is added to a structure with an amplitude approximated by comparing the rmsd between the measured and back-calculated rdcs using a correlation diagram similar to that shown in Figure 5.

The above approach for estimating error in order tensors determined for A-form helices (Aform-RDC) was validated using extensive computer simulations a subset of which is presented here. Sets containing 8, 11, 17, and 29 rdcs were tested using 100 theoretical structures each containing differing combinations of angular deviations with the scaling factor $L = 1.0$ and 1.5 Hz rdc error. Shown in Figure 6 are the average GDO and S_{zz} orientation errors obtained when fitting the rdcs to the ideal A-form geometry (open) and the error obtained using Aform-RDC (dashed). It is clear that on average the Aform-RDC derived errors are a very good estimate of the actual order tensor error. A more detailed analysis shows that the true GDO values were within the estimated error for 78%, 77%, 84%, and 81% of the cases examined. Likewise, the true S_{zz} orientation was within the estimated error for 83%, 96%, 88%, and 92% of the cases examined. As would be expected and can be seen in Figure 6 this method will often overestimate the order tensor error for smaller numbers of rdcs. This is due to the decreased correlation between the rdc(rmsd) and the order tensor error with decreasing N which leads to a larger range in the magnitude of possible error. The robustness of Aform-RDC for different levels of order tensor asymmetry (η) and S_{zz} orientation was also established on the basis of similar simulations (Supplementary material, Figure S3).

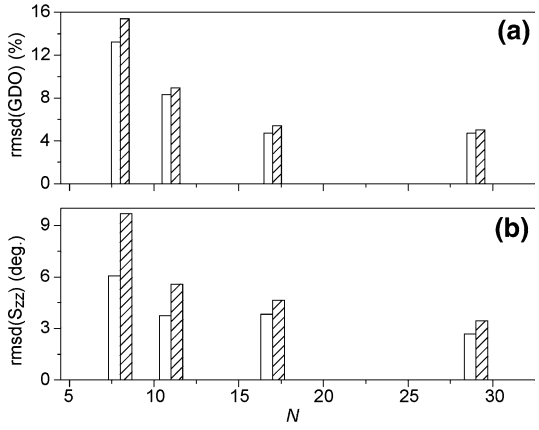

Figure 6. Estimating order tensor errors due to A-form angular deviations using 'Aform-RDC'. Shown are the error in the (a) GDO (rmsd(GDO)) and (b) S_{zz} orientation (rmsd(S_{zz})) for 8, 11, 17, and 29 rdcs obtained when fitting rdcs to an idealized A-from geometry in the presence of angular errors with the scaling factor $L = 1$ and 1.5 Hz rdc error (open) and the uncertainty estimated by Aform-RDC (dashed). Results are averages over 100 structures with 1.5 Hz rdc uncertainty and a starting order tensor of $S_{zz} = 0.001$ and $\eta = 0.20$.

Application of Aform-RDC in the error analysis of experimental rdcs measured in HIV-1 TAR RNA

We previously used the idealized A-form geometry (with improper propeller twist angles, see Materials and methods) in the order tensor analysis of rdcs measured in the two helices of HIV-1 TAR in free form (Al-Hashimi et al., 2002b) and bound to Mg^{2+} (Al-Hashimi et al., 2003) argininamide (Arg) (Pitt et al., 2004), the aminoglycoside neomycin B (NeoB) (Pitt et al., 2005), and the small molecule acetylpromazine (Acp) (Pitt et al., 2005). These studies together with previous NMR and X-ray structures of TAR (Puglisi et al., 1992; Aboul-ela et al., 1995; Ippolito and Steitz, 1998; Faber et al., 2000; Du et al., 2002) revealed a high degree of variability in the relative orientation and dynamics of the two TAR helices. For free TAR, the rdc analysis yielded an average inter-helical angle of $49° \pm 5°$ (Aboul-ela et al., 1996;

Al-Hashimi et al., 2002b). However, large differences in the helix GDOs provided evidence for large amplitude (±45°) inter-helical motions (Al-Hashimi et al., 2002b). A similar rdc analysis yielded a more linear and less flexible inter-helical angle for TAR bound to Mg^{2+} (Al-Hashimi et al., 2003), Arg (Puglisi et al., 1992; Aboul-ela et al., 1995; Pitt et al., 2004) and NeoB (Faber et al., 2000; Pitt et al., 2005). In contrast, the two helices remain bent and flexible when TAR is bound to the less positively charged small molecule Acp (Du et al., 2002; Pitt et al., 2005).

To assess the errors in the order tensor parameters, we re-analyzed the TAR rdcs using Aform-RDC. Results are summarized in Table 2. The estimated magnitude of angular deviations corresponded to scaling factors (L_{exp}) that ranged between 0.2 and 1.6 with 7 out of 10 helices exhibiting $L_{exp} < 1$. The $L_{exp} > 1$ value obtained for helix I of TAR-NeoB is consistent with the NMR structure of the complex which shows that NeoB binds and distorts the minor groove of helix I. The $L_{exp} > 1$ value observed for helix I in TAR-Mg(3:1) may reflect the small number of rdcs measured and possibly uncounted for rdc measurement error. Overall, the TAR helices fall within expectations based on our Gaussian A-form distribution.

The ratio of two helix GDOs (GDO_{int}) provides a lower-limit measure of inter-helix motional amplitudes (Tolman et al., 2001; Al-Hashimi et al., 2002b; Zhang et al., 2003). As shown in Table 2, the GDO_{int} ranges between 0.56 for free TAR to 0.99 for TAR-NeoB. The best-fit GDO_{int} values reported here differ slightly (by 5.4%, 1.6%, 3.3%, 3.1%, and 4.0% for TAR-Free, TAR-Acp, TAR-Arg, TAR-Mg, and TAR-NeoB, respectively) from those reported previously as some of the previous studies included rdcs from terminal residues and more importantly used an Insight II A-form helix geometry that has improper propeller twist angles. Similarly the differences in the inter-helical angles differ by 0°, 5°, 3°, 5°, and 12°, respectively. The larger difference observed for TAR-NeoB is not surprising given that the previous angle was calculated using the NMR structure for helix I.

Excluding TAR-Mg(3:1), the uncertainty in GDO_{int} estimated using Aform-RDC is < 8% and is on average ~5%. The smallest/largest errors are observed for TAR-Arg/TAR-Mg(3:1) for which the largest/smallest number of rdcs was measured. The larger error observed for TAR-Mg(3:1) (10.5%) also reflects larger rdc uncertainty arising from exchange broadening due to weak/non-specific Mg^{2+} binding (Al-Hashimi et al., 2003). Overall, the estimated errors in the GDO_{int} are significantly smaller than the range observed over the various liganded TAR states. Similarly, the estimated error in the S_{zz} orientation (< 8° and on average 4°) remains significantly smaller than the previously reported range of TAR inter-helical angles of (44°–0°).

Discussion

Determining the five order tensor elements for a rigid structural fragment is possible provided one has knowledge about how the rdc targeted bond vectors are oriented relative to one another. The achievable accuracy with which the order tensor elements can be determined is then dictated by the rdc uncertainty and accuracy with which the inter-nuclear vector orientation is known (Zweckstetter and Bax, 2002). However, only a subset of the total structural noise will propagate into order tensor errors. In our study, all translational deviations (such as slide, shift, and rise) within the A-form helix could be ignored since these do not affect the value of rdcs measured between directly bonded spins. Furthermore, not all structural (or dynamical) deviations that reorient rdc bonds will result in order tensor errors. Rather, no errors will be induced when the deviations lead to rotations around the rdc vector itself or maintain the rdc vector within the allowed two-fold set of taco-shaped orientations coded for by the 'real' order tensor (Ramirez and Bax, 1998).

The abundance and structural conservation across different contexts makes A-form helices ideal fragments for rdc-based characterization of RNA's global structural dynamics. In this work, we have examined how static and dynamical deviations from ideality affect the accuracy of derived order tensors. Results form our statistical survey of 232 Watson–Crick base-pairs in 40 unbound and ligand-bound RNA X-ray structures as well as analysis of 189 base-pairs from the 2.4 Å X-ray structure of the ribosome (Klein et al., 2001) (Supplementary material, Table S2) reinforce the validity of previously reported mean parameters

for the A-form RNA helix (Neidle, 1999). The experimental rdcs measured in the five TAR states as well as in other RNAs (Mollova et al., 2000; Sibille et al., 2001; Hansen and Al-Hashimi, 2006) provide experimental support for the validity the idealized geometry as a mean representation of RNA A-form helices in solution.

Our statistical survey of RNA X-ray structures allowed us to parameterize static deviations from the idealized A-form helix. Our simulation results suggest that while the order tensor errors in A-form helices will be dominated by such angular deviations, these errors are on average reasonably small for non-terminal Watson–Crick base-pairs, especially when having ≥11 rdcs. Although explored independently, it is very likely that some of the static A-form heterogeneity derived from comparison of solid state X-ray structures actually manifests as dynamical heterogeneity in solution that contributes to the observed ~7% uniform scaling of rdcs (Figure 1b). The latter motions correspond to isotropic cone motions (~18°) that are comparable in amplitude to the static deviations reported in Table 1. For this reason, the net order tensor errors reported here and shown in Figure 4 likely overestimate the real order tensor. Further studies are needed to characterize how correlations between the static deviations of different base and sugar moieties impact the determination of order tensors.

General use of the idealized A-form helix geometry is only possible if robust methods are available for estimating the order tensor error that can arise due to angular deviations and rdc uncertainty. The presented Aform-RDC procedure provides one robust approach for estimating the net order tensor error that is based on the quality of the rdc fit to the idealized A-form helix. This approach takes into account the particularities of the specific rdc set in hand and takes advantage of *a priori* knowledge regarding the A-form angular distribution. Although not presented, we were able to partially reduce the order tensor error by fitting rdcs to a range of noise corrupted A-form structures and choosing order tensor solutions that yield the best rdc fits (i.e. lowest rmsds). However, the improvements were only significant when having a large number of rdcs in which case the order tensor error was small to begin with or for cases in which the angular deviations were substantially larger than those documented in Table 1.

In conclusion, our study indicates that Watson–Crick helices in RNA provide 'molecular beacons' for characterizing the global conformational dynamics of both free and ligand-bound RNAs using rdcs. We anticipate that this will make possible NMR studies of global conformational dynamics in extremely large RNAs as well as allow changes in conformational dynamics in response to different environmental stimuli to be characterized in a high throughput manner.

Supplementary material is available for results of simulations with varying S_{zz} orientation and η.

Electronic supplementary material is available in the online version of this article at http://dx.doi.org/10.1007/s10858-006-9087-9 accessible for authorized users.

Acknowledgements

We thank members of the Al-Hashimi lab especially Alex Hansen and Qi Zhang for insightful comments. The authors gratefully acknowledge the Michigan Economic Development Cooperation and the Michigan Technology Tri-Corridor for the support of the purchase 600 MHz spectrometer. CM acknowledges financial support from an NIH sponsored Molecular Biophysics Training Grant. IA acknowledges support from the NSF CAREER Award. HMA acknowledges support from NIH grant RO1 AI066975-01. All programs implemented in this work are available from hashimi@umich.edu.

References

Aboul-ela, F., Karn, J. and Varani, G. (1995) *J. Mol. Biol.*, **253**, 313–332.

Aboul-ela, F., Karn, J. and Varani, G. (1996) *Nucleic Acids Res.*, **24**, 3974–3981.

Al-Hashimi, H.M. (2005) *Chembiochem*, **6**, 1506–1519.

Al-Hashimi, H.M., Gorin, A., Majumdar, A., Gosser, Y. and Patel, D.J. (2002a) *J. Mol. Biol.*, **318**, 637–649.

Al-Hashimi, H.M., Gosser, Y., Gorin, A., Hu, W., Majumdar, A. and Patel, D.J. (2002b) *J. Mol. Biol.*, **315**, 95–102.

Al-Hashimi, H.M., Pitt, S.W., Majumdar, A., Xu, W. and Patel, D.J. (2003) *J. Mol. Biol.*, **329**, 867–873.

Berman, H.M., Olson, W.K., Beveridge, D.L., Westbrook, J., Gelbin, A., Demeny, T., Hsieh, S.H., Srinivasan, A.R. and Schneider, B. (1992) *Biophys. J.*, **63**, 751–759.

Boisbouvier, J., Bryce, D.L., O'Neil-Cabello, E., Nikonowicz, E.P. and Bax, A. (2004) *J. Biomol. NMR*, **30**, 287–301.
Bondensgaard, K., Mollova, E.T. and Pardi, A. (2002) *Biochemistry*, **41**, 11532–11542.
Brooks, C.L. and Karplus, M. (1983) *J. Chem. Phys.*, **79**, 6312–6325.
Bruschweiler, R. (2003) *Curr. Opin. Struct. Biol.*, **13**, 175–183.
Bryce, D.L., Boisbouvier, J. and Bax, A. (2004) *J. Am. Chem. Soc.*, **126**, 10820–10821.
Cornell, W.D., Cieplak, P., Bayly, C.I., Gould, I.R., Merz, K.M., Ferguson, D.M., Spellmeyer, D.C., Fox, T., Caldwell, J.W. and Kollman, P.A. (1995) *J. Am. Chem. Soc.*, **117**, 5179–5197.
Dickerson, R.E. (1988) *Nucleic Acids Res*, **17**(5) 1797–1803.
Du, Z., Lind, K.E. and James, T.L. (2002) *Chem. Biol.*, **9**, 707–712.
Duchardt, E. and Schwalbe, H. (2005) *J. Biomol. NMR*, **32**, 295–308.
Faber, C., Sticht, H., Schweimer, K. and Rosch, P. (2000) *J. Biol. Chem.*, **275**, 20660–20666.
Gelbin, A., Schneider, B., Clowney, L., Hsieh, S.H., Olson, W.K. and Berman, H.M. (1996) *J. Am. Chem. Soc.*, **118**, 519–529.
Hansen, A.L. and Al-Hashimi, H.M. (2006) *J. Magn. Reson.*, **179**, 299–307.
Hoover, W.G. (1985) *Phys. Rev. A*, **31**, 1695–1697.
Ippolito, J.A. and Steitz, T.A. (1998) *Proc. Natl. Acad. Sci. USA*, **95**, 9819–9824.
Jaroniec, C.P., Boisbouvier, J., Tworowska, I., Nikonowicz, E.P. and Bax, A. (2005) *J. Biomol. NMR*, **31**, 231–241.
Jorgensen, W.L., Chandrasekhar, J., Madura, J.D., Impey, R.W. and Klein, M.L. (1983) *J. Chem. Phys.*, **79**, 926–935.
Klein, D.J., Schmeing, T.M., Moore, P.B. and Steitz, T.A. (2001) *EMBO J.*, **20**, 4214–4221.
Leulliot, N. and Varani, G. (2001) *Biochemistry*, **40**, 7947–7956.
Lilley, D.M. (2004) *Methods Mol. Biol.*, **252**, 77–108.
Lipari, G. and Szabo, A. (1982) *J. Am. Chem. Soc.*, **104**, 4546–4559.
Losonczi, J.A., Andrec, M., Fischer, M.W.F. and Prestegard, J.H. (1999) *J. Magn. Reson.*, **138**, 334–342.
Lu, X.J. and Olson, W.K. (2003) *Nucleic Acids Res.*, **31**, 5108–5121.
MacKerell, A.D., Banavali, N. and Foloppe, N. (2000) *Biopolymers*, **56**, 257–265.
McCallum, S.A. and Pardi, A. (2003) *J. Mol. Biol.*, **326**, 1037–1050.
Mollova, E.T., Hansen, M.R. and Pardi, A. (2000) *J. Am. Chem. Soc.*, **122**, 11561–11562.
Moore, P.B. (1999) *Annu. Rev. Biochem.*, **68**, 287–300.
Neidle, S. (1999) *Oxford Handbook of Nucleic Acid Structure*, Oxford University Press, New York.
Nose, S. (1984) *J. Chem. Phys.*, **81**, 511–519.
O'Neil-Cabello, E., Bryce, D.L., Nikonowicz, E.P. and Bax, A. (2004) *J. Am. Chem. Soc.*, **126**, 66–67.
Olson, W.K., Bansal, M., Burley, S.K., Dickerson, R.E., Gerstein, M., Harvey, S.C., Heinemann, U., Lu, X., Neidle, S., Sakked, Z., Sklenar, H., Suzuki, M., Tung, C., Weshof, E., Wolberger, C. and Berman, H.M. (2001) *J. Mol. Biol.*, **313**, 229–237.
Pitt, S.W., Majumdar, A., Serganov, A., Patel, D.J. and Al-Hashimi, H.M. (2004) *J. Mol. Biol.*, **338**, 7–16.
Pitt, S.W., Zhang, Q., Patel, D.J. and Al-Hashimi, H.M. (2005) *Angew. Chem. Int. Ed. Engl.*, **44**, 3412–3415.
Prestegard, J.H., Al-Hashimi, H.M. and Tolman, J.R. (2000) *Q. Rev. Biophys.*, **33**, 371–424.
Puglisi, J.D., Tan, R., Calnan, B.J., Frankel, A.D. and Williamson, J.R. (1992) *Science*, **257**, 76–80.
Ramirez, B.E. and Bax, A. (1998) *J. Am. Chem. Soc.*, **120**, 9106–9107.
Reiter, N.J., Blad, H., Abildgaard, F. and Butcher, S.E. (2004) *Biochemistry*, **43**, 13739–13747.
Saupe, A. (1968) *Angew. Chem. Int. Ed. Engl.*, **7**, 97–112.
Shajani, Z. and Varani, G. (2005) *J. Mol. Biol.*, **349**, 699–715.
Showalter, S.A., Baker, N.A., Tang, C.G. and Hall, K. (2005) *J. Biomol. NMR*, **32**, 179–193.
Sibille, N., Pardi, A., Simorre, J.P. and Blackledge, M. (2001) *J. Am. Chem. Soc.*, **123**, 12135–12146.
Sun, G., Voigt, J.H., Filippov, I.V., Marquez, V.E. and Nicklaus, M.C. (2004) *J. Chem. Inform. Comput. Sci.*, **44**, 1752–1762.
Tjandra, N. and Bax, A. (1997) *Science*, **278**, 1111–1114.
Tolman, J.R., Al-Hashimi, H.M., Kay, L.E. and Prestegard, J.H. (2001) *J. Am. Chem. Soc.*, **123**, 1416–1424.
Tolman, J.R., Flanagan, J.M., Kennedy, M.A. and Prestegard, J.H. (1995) *Proc. Natl. Acad. Sci. USA*, **92**, 9279–9283.
Tolman, J.R., Flanagan, J.M., Kennedy, M.A. and Prestegard, J.H. (1997) *Nat. Struct. Biol.*, **4**, 292–297.
Trantirek, L., Urbasek, M., Stefl, R., Feigon, J. and Sklenar, V. (2000) *J. Am. Chem. Soc.*, **122**, 10454–10455.
Vallurupalli, P. and Kay, L.E. (2005) *J. Am. Chem. Soc.*, **127**, 6893–6901.
van Buuren, B.N., Schleucher, J., Wittmann, V., Griesinger, C., Schwalbe, H. and Wijmenga, S.S. (2004) *Angew. Chem. Int. Ed. Engl.*, **43**, 187–192.
Warren, J.J. and Moore, P.B. (2001) *J. Biomol. NMR*, **20**, 311–323.
Zhang, Q., Sun, X., Watt, E.D. and Al-Hashimi, H.M. (2006) *Science*, **311**, 653–656.
Zhang, Q., Throolin, R., Pitt, S.W., Serganov, A. and Al-Hashimi, H.M. (2003) *J. Am. Chem. Soc*, **125**, 10530–10531.
Zweckstetter, M. (2003) *J. Biomol. NMR*, **27**, 41–56.
Zweckstetter, M. and Bax, A. (2002) *J. Biomol. NMR*, **23**, 127–137.